SCIENTIFIC REPORTS

OPEN

SUBJECT AREAS:
ACUTE INFLAMMATION
TRANSCRIPTION
INFECTION
TARGET IDENTIFICATION

Received
7 August 2012

Accepted
6 November 2012

Published
28 January 2013

Correspondence and requests for materials should be addressed to Y.C.L. (leeyc@jbnu.ac.kr)

* These authors contributed equally to this work.

Inhibition of endoplasmic reticulum stress alleviates lipopolysaccharide-induced lung inflammation through modulation of NF-κB/HIF-1α signaling pathway

Hee Jung Kim[1,3]*, Jae Seok Jeong[1,3]*, So Ri Kim[1,3]*, Seung Yong Park[1,3], Han Jung Chae[2,3] & Yong Chul Lee[1,3]

[1]Department of Internal Medicine, [2]Department of Pharmacology, [3]Research Center for Pulmonary Disorders, Chonbuk National University Medical School, Jeonju, South Korea.

Lipopolysaccharide (LPS) is involved in a variety of inflammatory disorders. Under stress conditions, endoplasmic reticulum (ER) loses the homeostasis in its functions, which is defined as ER stress. Little is known how ER stress is implicated in LPS-induced lung inflammation. In this study, effects of inhibition of ER stress on LPS-induced lung inflammation and transcriptional regulation were examined. An ER stress regulator, 4-phenylbutyrate (PBA) reduced LPS-induced increases of various ER stress markers in the lung. Furthermore, inhibition of ER stress reduced the LPS-induced lung inflammation. Moreover, LPS-induced increases of NF-κB and HIF-1α activity were lowered by inhibition of ER stress. These results suggest that inhibition of ER stress ameliorates LPS-induced lung inflammation through modulation of NF-κB/IκB and HIF-1α signaling pathway.

Lipopolysaccharide (LPS), a primary component of endotoxin of Gram-negative bacteria cell walls, is commonly associated with a variety of human disorders including acute lung injury (ALI) that leads to severe inflammation by activating various inflammatory cells[1]. Nuclear factor (NF)-κB is activated by LPS and regulates many pro-inflammatory mediators thought to be important for establishing of lung inflammation/injury[2,3]. In addition, LPS also induces hypoxia-inducible factor (HIF)-1α[4], which modulates inflammation and plasma exudation through the regulation of vascular endothelial growth factor (VEGF) expression in pulmonary inflammatory disorders[5]. However, the molecular mechanism by which LPS mounts inflammatory processes in the lung remains unknown.

Endoplasmic reticulum (ER) stress is defined as accumulation of unfolded or misfolded proteins in the ER, a subcellular organelle mainly known as a protein-folding factory[6–9]. There are three ER-localized protein sensors for ER stress: inositol-requiring enzyme 1α (IRE1α), double-stranded RNA-dependent protein kinase (PKR)-like ER kinase (PERK), and activating transcription factor (ATF)-6. When these sensors recognize the enhanced ER stress, they activate the unfolded-protein response (UPR) processes such as the increases of expression of glucose-regulated protein 78 (GRP78) and CCAAT/enhancer-binding protein-homologous protein (CHOP). GRP78 is a prominent ER-resident chaperone, which binds to these three ER stress sensors, but more stably interacts with misfolded or unfolded proteins[6]. Therefore, up-regulation of GRP78 is used as an ER stress marker most commonly[10]. In addition, CHOP, an apoptotic transcriptional factor induced in response to ER stress, is also a popular marker for assessment of ER stress[11]. Numerous studies have demonstrated that ER stress is involved in various disorders including neurodegenerative disorders, metabolic disorders, inflammatory diseases, and malignancies[7–9]. In addition, ER stress may play a role in LPS-induced lung inflammation[11,12]. However, little is known regarding the mechanism by which ER stress is implicated in LPS-induced lung inflammation, especially transcriptional regulations for pro-inflammatory gene expression.

In this study, we used both *in vitro* (a human lung epithelial cell line) and *in vivo* (a mouse model of LPS-induced lung inflammation) experimental systems to examine an involvement of ER stress and the related molecular mechanisms associated with ER stress in LPS-induced lung inflammation. In addition, we also ensured the association of ER stress with human lung inflammation/injury by measuring the levels of GRP78 and CHOP.

Results

ER stress markers are increased in lung tissues of LPS-treated mice and peripheral blood mononuclear cells (PBMCs) from patients with severe lung inflammation. To evaluate whether ER stress is involved in LPS-induced lung inflammation, we determined levels of GRP78 and CHOP protein in lung tissues from LPS-treated mice. The level of GRP78 was increased approximately 2.69-, 3.34-, 3.22-, 3.36- and 3.65-fold at 6, 12, 36, 48, and 72 hours after administration of LPS, respectively, compared with the pretreatment period (**Fig. 1a,b**). The level of CHOP was also increased approximately 2.05-, 2.31-, 2.34-, 3.66-, and 3.43-fold at 6, 12, 36, 48, and 72 hours after administration of LPS, respectively, compared with the pretreatment period (**Fig. 1c,d**).

4-phenylbutyrate (4-PBA) lowers LPS-induced increases of GRP78 and CHOP protein in lung tissues and in normal human bronchial epithelial (NHBE) cells. To ascertain the observations that GRP78 and CHOP were increased in lung tissues of LPS-treated mice, these proteins were visualized by immunofluorecence staining (**Fig. 2a**). Confocal microscopic analyses revealed that immunofluorescence staining of GRP78 and CHOP was markedly increased at 48 hours after LPS treatment, especially in bronchiolar epithelium and inflammatory cells around bronchioles compared with 0.9% NaCl solution-treated mice. Administration of 4-PBA substantially reduced the increases of immunofluorescence staining of GRP78 and CHOP in lung tissues of LPS-treated mice.

In addition, Western blot analyses revealed that the LPS-induced increases of GRP78 and CHOP protein in lung tissues were significantly reduced by administration of 4-PBA (**Fig. 2b–e**). Consistent with these results, in LPS-treated NHBE cells, levels of GRP78 and CHOP protein were significantly increased at 12 hours after LPS treatment. Pre-treatment with 4-PBA significantly inhibited the LPS-induced increases of GRP78 and CHOP protein in NHBE cells (**Fig. 2f–i**).

4-PBA reduces increases of UPR-related proteins in lung tissues of LPS-treated mice. To investigate effects of 4-PBA on UPR-related markers, we measured levels of X-box binding protein-1 (XBP-1), ATF-6, ATF-4, and phosphorylation of eukaryotic initiation factor 2 alpha (eIF2α) in lung tissues of LPS-treated mice. Western blot analyses showed that the levels of XBP-1, ATF-6, and ATF-4 in nuclear protein extracts from lung tissues were significantly increased at 48 hours after LPS treatment as compared with 0.9% NaCl solution–treated mice. The increases of XBP-1, ATF-6, and ATF-4 protein in the LPS-treated mice were substantially reduced by administration of 4-PBA (**Fig. 3a–f**). The level of phospho-eIF2α in lung tissues was increased at 48 hours after LPS treatment compared with the level in 0.9% NaCl solution-treated mice. The increase of phospho-eIF2α in the LPS-treated mice was markedly reduced by administration of 4-PBA (**Fig. 3g,h**). However, no significant changes in eIF2α levels were observed in any of the groups tested.

Inhibition of ER stress attenuates LPS-induced lung inflammation and plasma exudation in mice. In LPS-treated mice, we could find significant increases in numbers of total cells, macrophages, lymphocytes, and neutrophils in BAL fluids. Moreover, plasma exudation and level of total protein in BAL fluids were also increased. The increase in numbers of these cells, especially neutrophils, and the level of total protein in BAL fluids was significantly reduced by administration of 4-PBA (**Fig. 4a–c**). In addition, histological analyses showed a marked infiltration of inflammatory cells into the alveolar space, peribronchial wall thickening, and vascular congestion. Administration of 4-PBA resulted in a substantial reduction of the LPS-induced infiltration of inflammatory cells into the alveolar space, peribronchial area, and vascular congestion in the lung of mice (**Fig. 4d**).

On micro-CT scan, LPS-treated mice showed bilateral diffuse ground glass opacities with the prominent bronchovascular bundle and bronchial wall thickenings in both lung fields, contrast to the findings of 0.9% NaCl solution-treated mice (**Fig. 4d**). Administration of 4-PBA restored the radiologic changes occurred by LPS treatment, to some degree, toward the findings of 0.9% NaCl solution-treated mice.

Inhibition of ER stress lowers increases of pro-inflammatory proteins in lung of LPS-treated mice. To assess the role of ER stress in LPS-induced production of pro-inflammatory mediators in lung inflammation, we measured the level of IFN-γ, TNF-α,

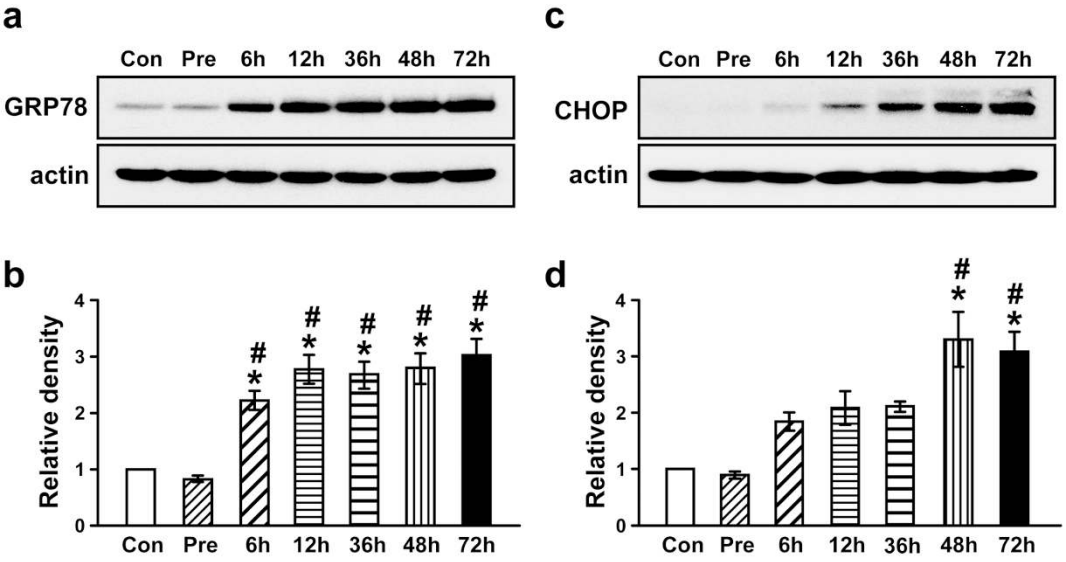

Figure 1 | The levels of ER stress markers in lung tissues of LPS-treated mice and in PBMCs from patients with severe lung inflammation and healthy subjects. Western blot analyses of GRP78 (a) and CHOP (c) in lung tissues of LPS-treated mice. Analyses of band intensity on films are presented as the relative ratio of GRP78 (b) and CHOP (d) to actin. The relative ratio of each protein in the lung tissues of control mice is arbitrarily presented as 1. Six, 12, 36, 48, and 72 hours are the time periods of the sampling after treatment of mice with LPS. Bars represent mean ± SEM from 8 mice per group. Con, 0.9% NaCl solution (saline)-treated mice administered with drug vehicle; Pre, 1 hour before the LPS treatment. $^{*}P < 0.05$ versus Con. $^{\#}P < 0.05$ versus Pre.

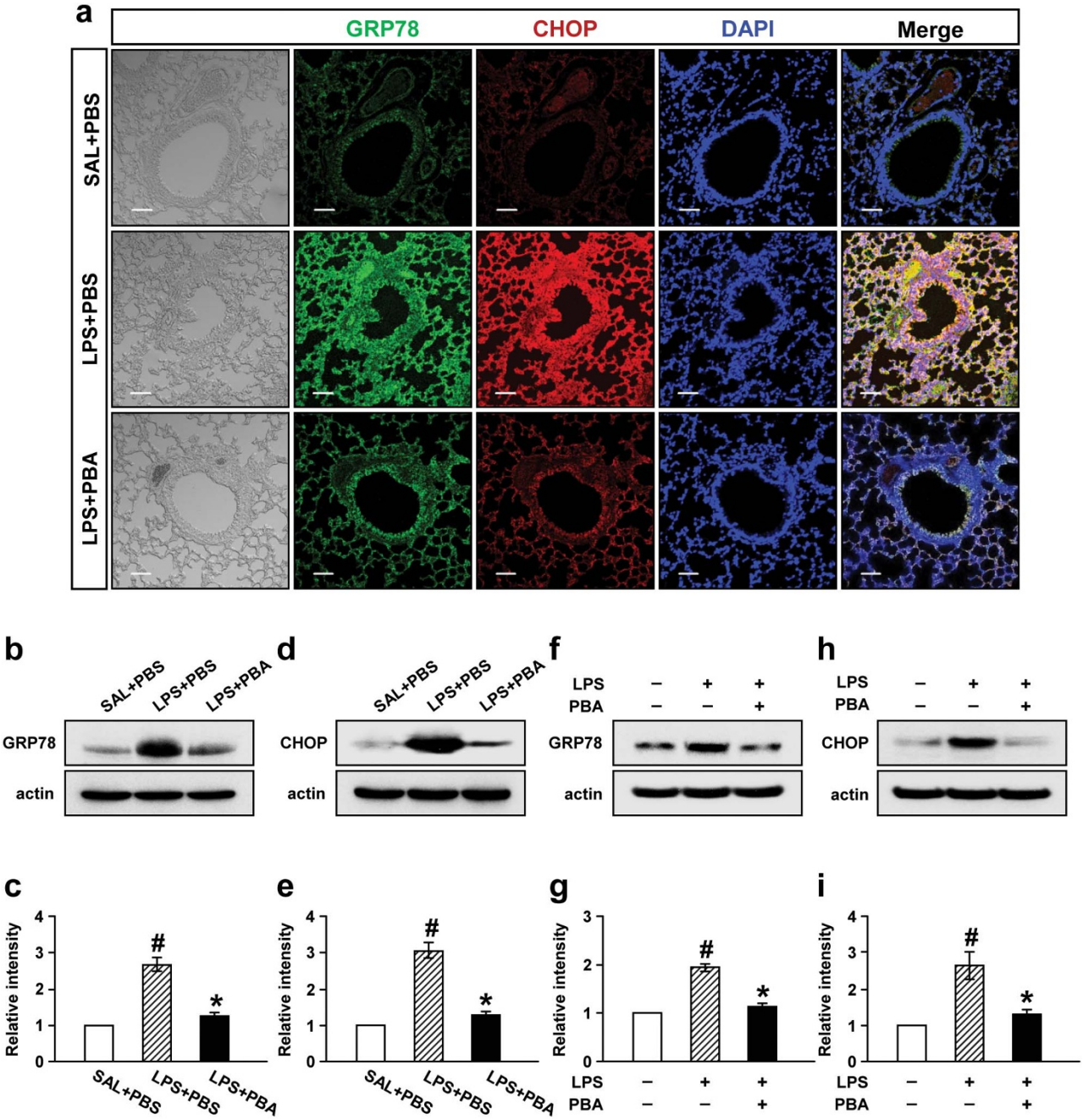

Figure 2 | Effect of 4-PBA on levels of GRP78 and CHOP protein in lung tissues of LPS-treated mice (a-e) and in LPS-stimulated NHBE cells (f-i). Sampling was performed at 48 hours after LPS treatment in 0.9% NaCl solution (saline)-treated mice administered with drug vehicle (PBS) (SAL+PBS), LPS-treated mice administered with PBS (LPS+PBS), or LPS-treated mice administered with 4-PBA (LPS+PBA). (a) Representative confocal immunofluorescence photomicrography showed the expression of GRP78 protein (the middle-left panels, green fluorescence views) and CHOP protein (the middle panels, red fluorescence views) in SAL+PBS (the upper panels), LPS+PBS (the center panels), or LPS+PBA (the bottom panels). Bars indicate scale of 50 μm. Representative Western blot analysis of GRP78 (b) and CHOP (d) in lung tissues of LPS-treated mice. Analyses of band intensity on films are presented as the relative ratio of GRP78 (c) and CHOP (e) to actin. The relative ratio of each protein in the lung tissues of SAL+PBS is arbitrarily presented as 1. Bars represent mean ± SEM from 8 mice per group. In NHBE cells, the protein levels were determined at 12 hours after treatment with LPS. Representative Western blot analysis of GRP78 (f) and CHOP (h) in NHBE cells. Analyses of band intensity on films are presented as the relative ratio of GRP78 (g) and CHOP (i) to actin. The relative ratio of each protein in NHBE cells with no treatment is arbitrarily presented as 1. Bars represent mean ± SEM from 3 independent experiments. $^{\#}P < 0.05$ versus SAL+PBS or no treatment; $^{*}P < 0.05$ versus LPS+PBS or treatment with LPS only.

IL-1β, intercellular adhesion molecule-1 (ICAM-1), chemokine CXCL1 (KC), and VEGF. Western blot analyses showed that levels of IFN-γ, TNF-α, IL-1β, and ICAM-1 protein in lung tissues were significantly increased at 48 hours after LPS treatment compared with the levels of 0.9% NaCl solution-treated mice (**Fig. 5a–h**). Administration of 4-PBA reduced significantly the LPS-induced increases of IFN-γ, TNF-α, IL-1β, and ICAM-1 protein in lung tissues.

As expected, the protein levels of KC (**Fig. 5i,j**) and VEGF (**Fig. 5k,l**) were also significantly increased in BAL fluids of

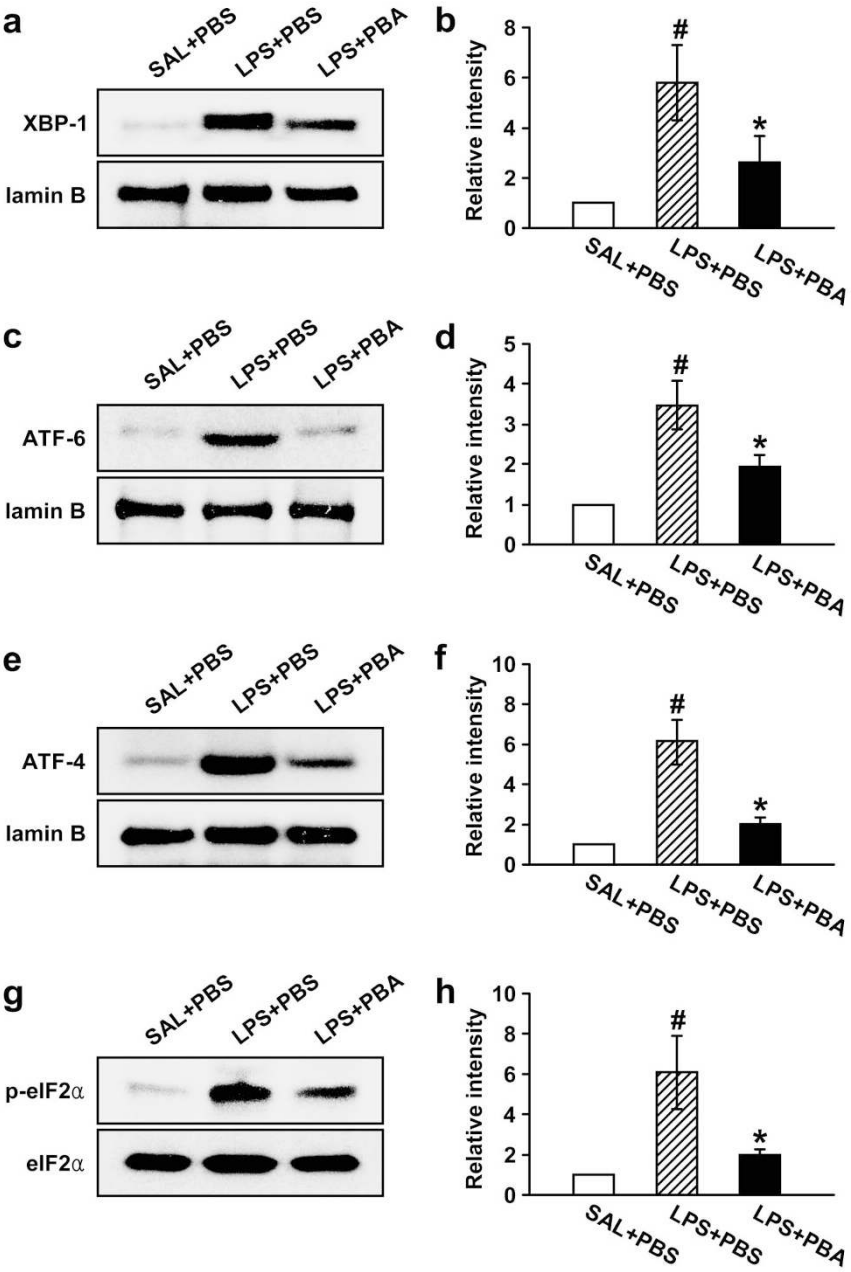

Figure 3 | Effects of 4-PBA on the levels of UPR-related markers in lung tissues of LPS-treated mice. Sampling was performed at 48 hours after the LPS treatment in 0.9% NaCl solution (saline)-treated mice administered with drug vehicle (PBS) (SAL+PBS), LPS-treated mice administered with PBS (LPS+PBS), or LPS-treated mice administered with 4-PBA (LPS+PBA). Representative Western blots of XBP-1 (a), ATF-6 (c), ATF-4 (e) and p-eIF2α (g) in lung tissues. Analyses of band intensity on films are presented as the relative ratio of XBP-1 (b), ATF-6 (d), and ATF-4 (f) proteins to lamin B. In case of p-eIF2α (h), the relative ratio was presented to eIF2α. The relative ratio of each protein in the lung tissues of SAL+PBS is arbitrarily presented as 1. Bars represent mean ± SEM from 8 mice per group. $^{\#}P < 0.05$ versus SAL+PBS; $^{*}P < 0.05$ versus LPS+PBS.

LPS-treated mice, and administration of 4-PBA reduced the increases of these protein levels.

Inhibition of ER stress reduces nuclear translocation of NF-κB p65 and degradation of inhibitor of NF-κB α (IκBα) protein in lung tissues of LPS-treated mice. In Western blotting data, the level of NF-κB p65 in nuclear protein extracts of lung tissues was significantly increased at 48 hours after LPS treatment compared with the level in 0.9% NaCl solution-treated mice. The LPS-induced increase of nuclear NF-κB p65 was significantly decreased by administration of 4-PBA (**Fig. 6a,b**). Accordingly, the level of NF-κB p65 in cytosolic protein fractions of lung tissues was decreased after LPS treatment compared with the level in 0.9% NaCl solution-treated mice. The LPS-induced decrease of cytosolic NF-κB p65 was substantially restored by administration of 4-PBA. The level of IκBα protein in lung tissues was significantly decreased at 48 hours after LPS treatment compared with the level in 0.9% NaCl solution-treated mice (**Fig. 6c,d**). The LPS-induced decrease of IκBα protein was significantly blocked by administration of 4-PBA.

Inhibition of ER stress lowers level of HIF-1α protein in lung tissues of LPS-treated mice. The protein level of HIF-1α, which leads to VEGF expression, was determined by Western blotting. The level of HIF-1α in lung tissues of LPS-treated mice was markedly increased at 48 hours after LPS treatment compared with the level in 0.9% NaCl solution-treated mice (**Fig. 6e,f**). The

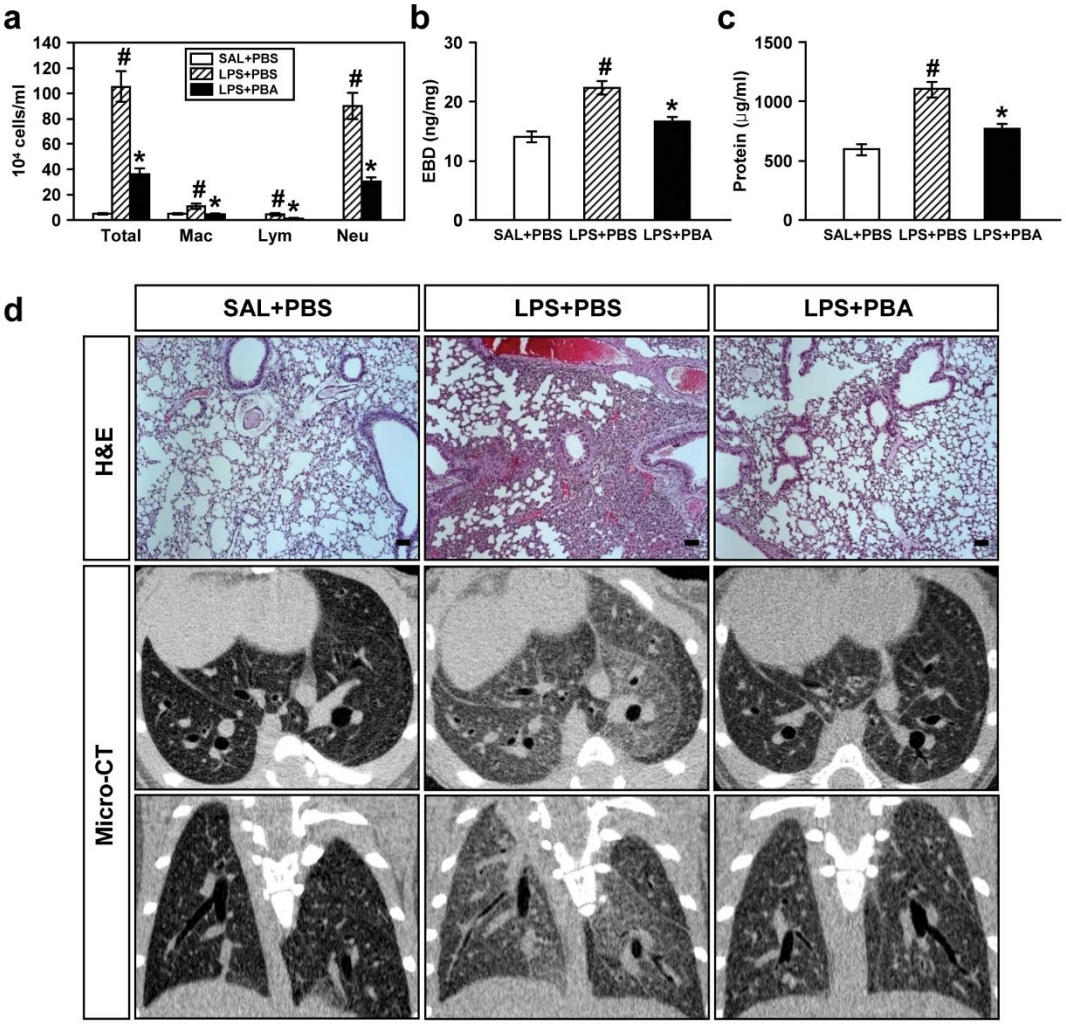

Figure 4 | Effects of 4-PBA on the differential cellular components (a), plasma exudation using EBD assay (b), total protein amounts (c) in BAL fluids, and pathologic and radiologic changes (d) of LPS-treated mice. All parameters were measured at 48 hours after LPS treatment in 0.9% NaCl solution (saline)-treated mice administered with drug vehicle (PBS) (SAL+PBS), LPS-treated mice administered with PBS (LPS+PBS), or LPS-treated mice administered with 4-PBA (LPS+PBA). Bars represent mean ± SEM from 8 mice per group in (a-c). $^{\#}P < 0.05$ versus SAL+PBS; $^{*}P < 0.05$ versus LPS+PBS. (d) Representative H&E stained sections of the lungs isolated from SAL+PBS, LPS+PBS, and LPS+PBA. Bars indicate 50 μm. As for the micro-CT scan images, representative transaxial images (the upper panels) and coronal images (the bottom panels).

LPS-induced increase of HIF-1α was significantly reduced by administration of 4-PBA. However, the level of HIF-1β protein was not changed in any groups tested.

GRP78 RNA interference reduces the expression of GRP78 and the nuclear translocation of NF-κB in LPS-treated NHBE cells. To examine whether ER stress influences on NF-κB activation, an ER stress protein, GRP78 was knockdown in LPS-treated cells using GRP78 siRNA. Western blot analysis showed that level of GRP78 protein in LPS-treated NHBE cells was significantly decreased by treatment with GRP78 siRNA. Moreover, the LPS-induced increase of nuclear NF-κB p65 was significantly decreased by GRP78 siRNA restoring LPS-induced decrease of cytosolic NF-κB p65 almost up to the level in LPS-untreated cells (**Fig. 7**).

ER stress is enhanced in PBMCs isolated from the patients with acute lung injury. To evaluate an involvement of ER stress in human lung inflammation, we determined the protein levels of GRP78 and CHOP using PBMCs obtained from patients with severe lung inflammation and healthy subjects (**supplementary Table 1**). Western blot analyses showed that the levels of GRP78 and CHOP were increased significantly in patients with severe lung inflammation compared with those in healthy subjects (**Fig. 8**).

Discussion

Current study has demonstrated that ER stress is implicated in the pathogenesis of LPS-induced lung inflammation through transcriptional regulation including NF-κB and HIF-1α pathway and provides a novel promising therapeutic target for pulmonary inflammatory disorders.

Accumulating evidence has suggested that ER stress is associated with a variety of diseases including obesity, diabetes, atherosclerosis, neurodegenerative diseases, cancer, and inflammatory diseases[7–10]. In particular, some pulmonary disorders have been shown to associate with enhancement of ER stress[13,14]. ER stress-induced cytotoxicity is implicated in the pathogenesis of chronic obstructive pulmonary disease (COPD)[13]. In case of idiopathic pulmonary fibrosis, the apoptosis of type II alveolar epithelial cells, the key pathologic mechanism, is induced by severe ER stress[14]. Consistent with these observations, our results showed that levels of GRP78 and CHOP protein were significantly increased in lung tissues of LPS-treated mice and in LPS-treated NHBE cells. UPR-related markers including ATF-6,

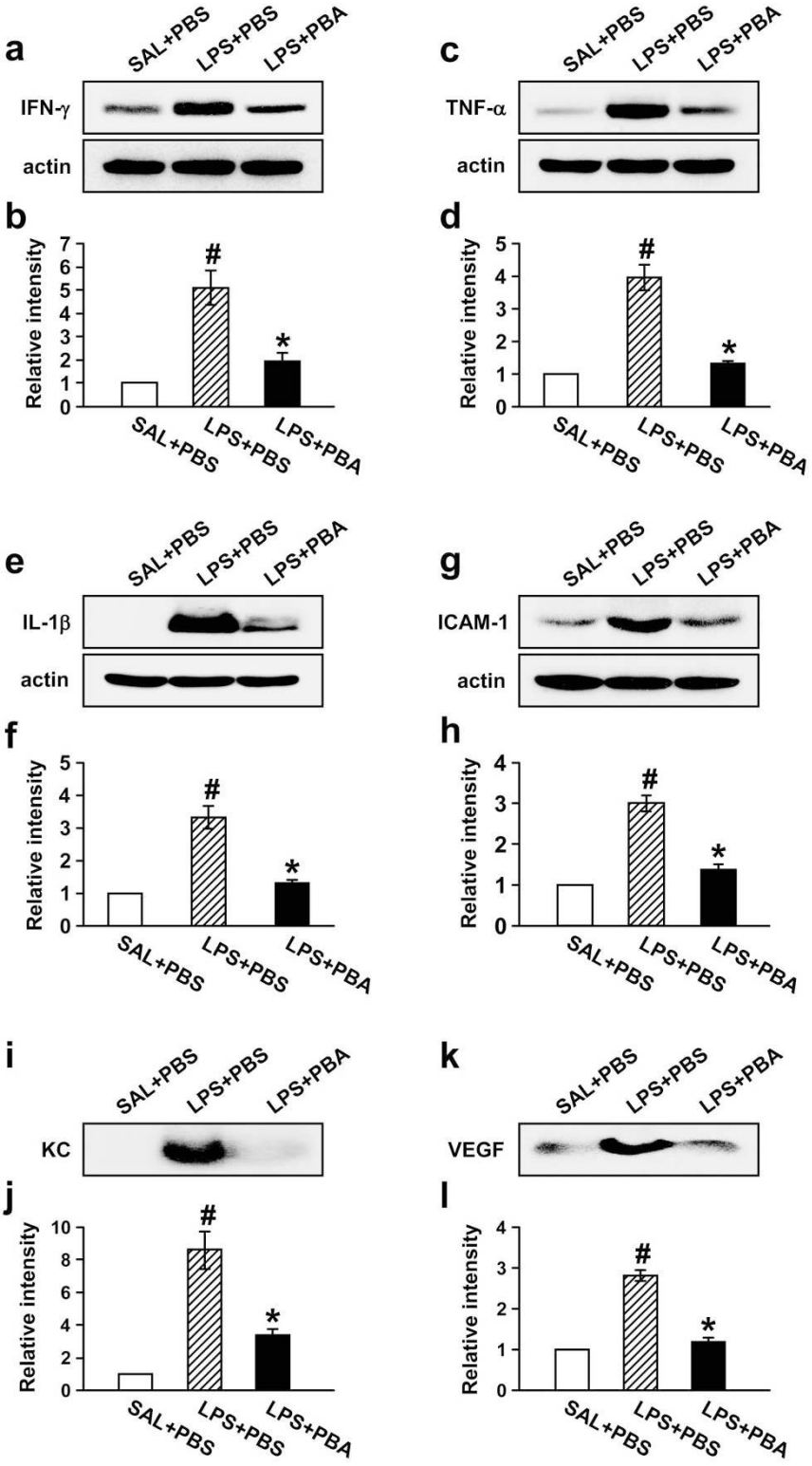

Figure 5 | Effects of 4-PBA on the levels of IFN-γ, TNF-α, IL-1β, ICAM-1, KC, and VEGF protein in lung of LPS-treated mice. Sampling was performed at 48 hours after LPS treatment in 0.9% NaCl solution (saline)-treated mice administered with drug vehicle (PBS) (SAL+PBS), LPS-treated mice administered with PBS (LPS+PBS), or LPS-treated mice administered with 4-PBA (LPS+PBA). Representative Western blots of IFN-γ (a), TNF-α (c), IL-1β (e), and ICAM-1 (g) in the lung tissues and of KC (i) and VEGF (k) in the BAL fluids. Analyses of band intensity on films are presented as the relative ratio of IFN-γ (b), TNF-α (d), IL-1β (f), and ICAM-1 (h) to actin, while in case of KC and VEGF, analyses of band intensity on films are presented as the relative ratio of the level of KC (j) and VEGF (l) in each group to the level in SAL+PBS. The relative ratio of each protein in the lung tissues of SAL+PBS is arbitrarily presented as 1. Bars represent mean ± SEM from 8 mice per group. $^{\#}P < 0.05$ versus SAL+PBS; $^{*}P < 0.05$ versus LPS+PBS.

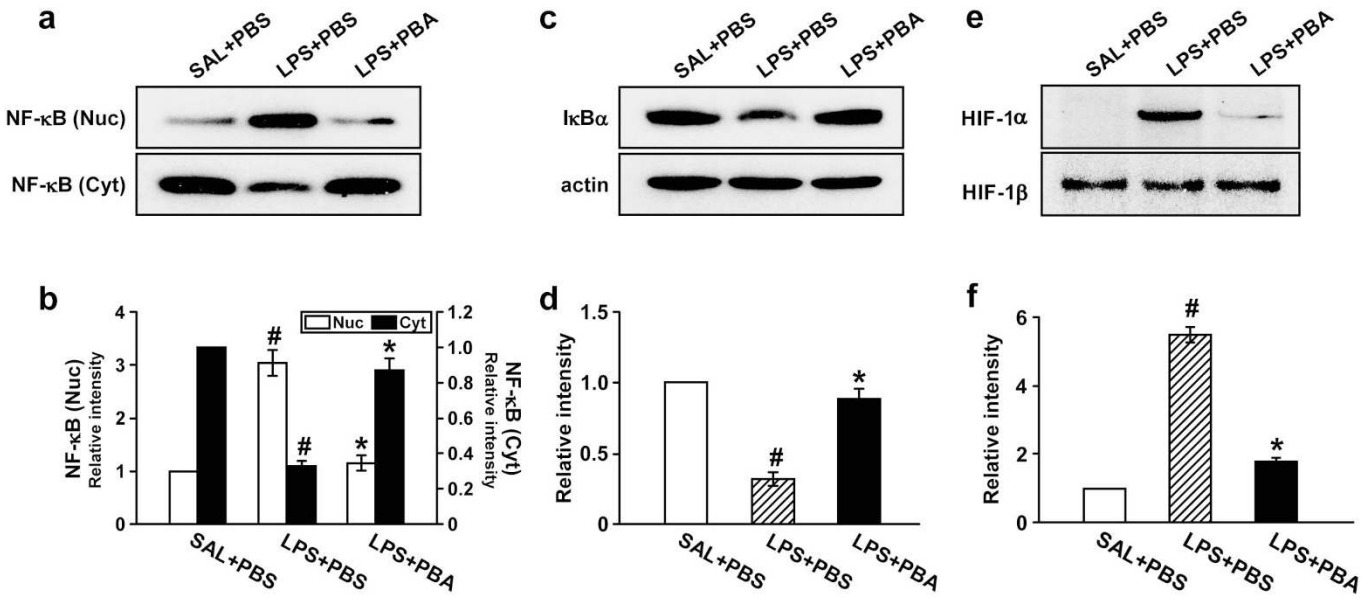

Figure 6 | Effects of 4-PBA on the activations of NF-κB/IκBα p65 and on the HIF-1α protein levels in lung tissues of LPS-treated mice. Sampling was performed at 48 hours after LPS treatment in 0.9% NaCl solution (saline)-treated mice administered with drug vehicle (PBS) (SAL+PBS), LPS-treated mice administered with PBS (LPS+PBS), or LPS-treated mice administered with 4-PBA (LPS+PBA). Representative Western blots of NF-κB p65 (a) and IκBα (c) in the lung tissues. (b) Analyses of band intensity on films are presented as the relative ratio of the level of NF-κB p65 in each group to the level in SAL+PBS. (d) In case of IκBα, the relative ratio was presented to actin. The relative ratio of each protein in the lung tissues of SAL+PBS is arbitrarily presented as 1. (e) Representative Western blots of HIF-1α and HIF-1β in nuclear protein extracts from the lung tissues. (f) Analyses of band intensity on films are presented as the relative ratio of HIF-1α to HIF-1β in LPS+PBS or LPS+PBA to those in SAL+PBS. The relative ratio of each protein in the lung tissues of SAL+PBS is arbitrarily presented as 1. Bars represent mean ± SEM from 8 mice per group. $^{\#}P < 0.05$ versus SAL+PBS; $^{*}P < 0.05$ versus LPS+PBS.

XBP-1, phospho-eIF2α, and ATF-4 were also significantly elevated in lung tissues of LPS-treated mice. Moreover, the level of GRP78 and CHOP protein in PBMCs obtained from patients with severe lung inflammation was significantly higher than the level in healthy subjects. Furthermore, we have found that 4-PBA, which is a potent ER stress inhibitor, markedly reduced the LPS-induced up-regulation of GRP78, CHOP, and UPR-related markers in mice. These LPS-induced changes in GRP78 and CHOP level were further supported by immunofluorescence staining. These findings suggest that ER stress is one of the crucial players during inducing and maintaining of LPS-induced lung inflammation and that 4-PBA attenuates ER stress in this pathologic condition.

Recently, a number of investigators have reported that suppression of ER stress stabilizes protein conformation, facilitates the trafficking of mutant proteins, and improves ER folding capacity and that ER stress is a potential therapeutic target for various diseases including diabetes, cystic fibrosis, and ischemic injuries of brain, spinal cords and liver[10,15–21]. In the present study, blocking of ER stress markedly reduced the LPS-induced increase of airway inflammatory cells, inflammatory mediators, vascular congestion, and

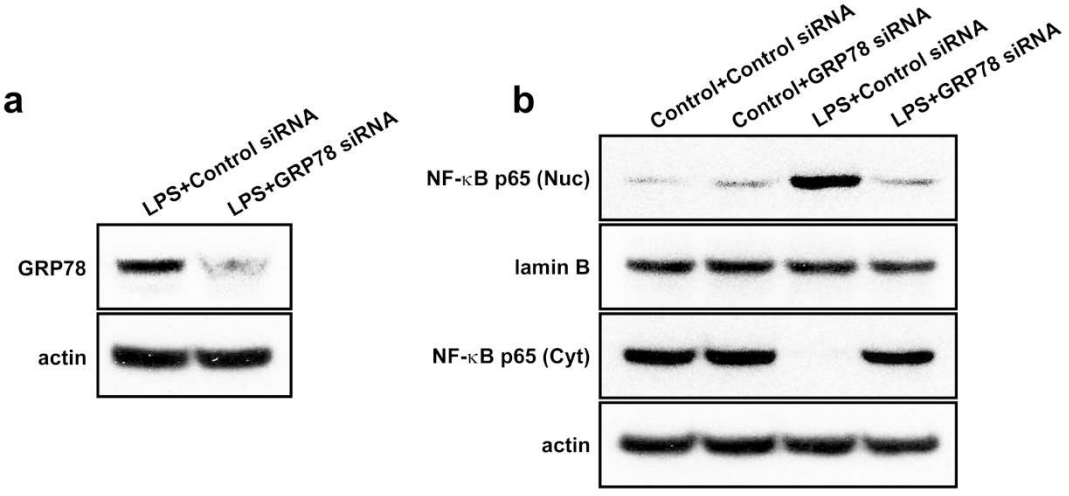

Figure 7 | Effects of GRP78 RNA interference on the protein expression of GRP78 and NF-κB activation in LPS-treated NHBE cells. (a) Western blot analysis of GRP78 in LPS-treated NHBE cells. (b) Western blotting of NF-κB p65 in nuclear (Nuc) and cytosolic (Cyt) extracts from NHBE cells treated with LPS or co-treated with LPS and GRP78 siRNA.

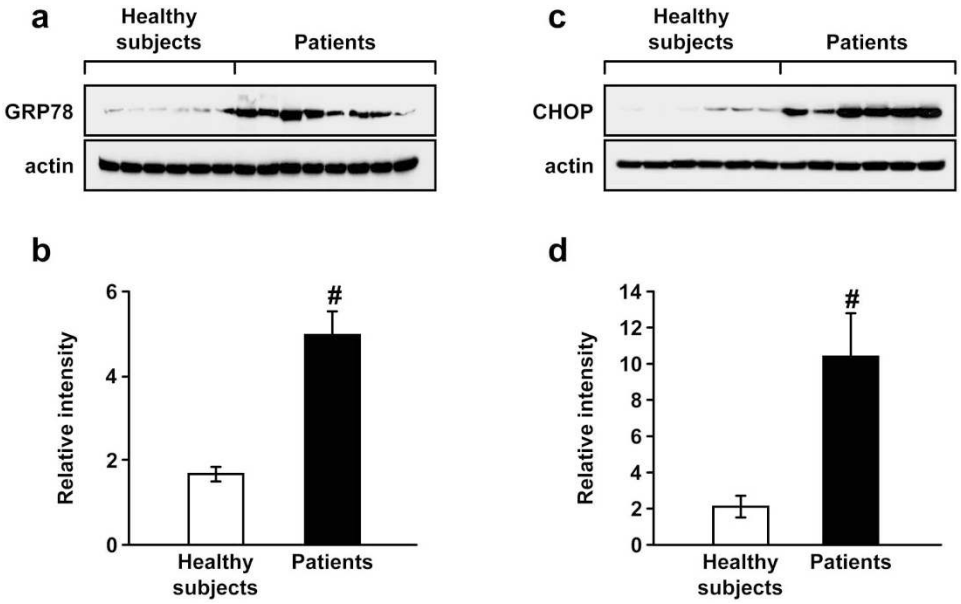

Figure 8 | The protein levels of GRP78 and CHOP in PBMCs from patients with ALI. Western blot analysis of GRP78 (a) and CHOP (c). Protein levels were determined using protein extracts of PBMCs obtained from healthy subjects as well as patients with ALI. Analyses of band intensity on films are presented as the relative ratio of GRP78 (b) or CHOP (d) to actin. The relative ratio of GRP78 or CHOP in the first healthy subject (i.e., 1st left lane) is arbitrarily standardized as 1. Bars represent mean ± SEM from each group. $^{\#}P < 0.05$ versus healthy subjects.

plasma exudation in the lung of mice. Through micro-CT scanning, we have ascertained that inhibition of ER stress attenuates the LPS-induced abnormal radiologic findings such as increased ground glass opacities and prominent bronchovascular bundles. Taken together, we suggest that inhibition of ER stress significantly ameliorates pulmonary inflammation and plasma exudation in LPS-induced lung inflammation.

Additionally, based on our current results, we can speculate two possible molecular mechanisms by which ER stress regulates airway inflammation and plasma exudation in LPS-induced lung inflammation.

First, ER stress regulates NF-κB signaling pathway in LPS-induced lung inflammation. NF-κB is known as a key transcription regulator that has a central role in immune response and inflammation[22]. Moreover, ER stress is involved in various inflammatory processes partly through the regulation of NF-κB[8,9]. In the current study, the degradation of IκBα was significantly increased by LPS treatment, resulting in nuclear translocation of NF-κB. The levels of inflammatory mediators including TNF-α, IL-1β, KC, ICAM, and VEGF, which are known to be dependent on NF-κB pathway[3,23,24], were increased by the LPS treatment. Moreover, in case of airway inflammation, we have previously reported that expression of adhesion molecule, chemokines, and cytokines is regulated through activation of NF-κB in airway inflammatory disorders[25]. Of note, in the present study, inhibition of ER stress blocked the increase in nuclear translocation of NF-κB p65 and degradation of IκBα which lead to inhibit the expression of various inflammatory mediators. In addition, LPS-induced increase in the levels of pro-inflammatory mediators in the lung was significantly reduced by the blocking of ER stress using 4-PBA. These findings suggest that ER stress is closely associated with the expression of various inflammatory mediators through regulation of NF-κB/IκBα signaling pathway in LPS-induced lung inflammation.

Second, ER stress is also linked to the HIF-1α signaling pathway in LPS-induced lung inflammation. While classically HIF-1α is known to enhance cellular adaptation to hypoxia through transcription of genes such as VEGF, EPO, and several glycolytic enzymes[26], recently it has uncovered that HIF-1α plays an important role in immune and inflammatory responses independent of cellular oxygen status[27,28]. In addition, HIF-1α is involved in ER stress pathways[29,30]. In this study, HIF-1α activity as well as the level of VEGF protein was increased in the lung of LPS-treated mice. VEGF is one of the target genes of HIF-1α, enhances microvascular permeability, and plays a key role in airway inflammation[5,31,32]. Our data also showed that inhibition of ER stress significantly reduced the activity of HIF-1α, production of VEGF, and plasma exudation accompanying pulmonary inflammation/injury in the lung of LPS-treated mice. These observations indicate that inhibition of ER stress may improve plasma exudation by suppression of the expression of various inflammatory mediators, in particular, VEGF induced by HIF-1α activation in LPS-induced lung inflammation. Taken together, ER stress regulates lung inflammation and plasma exudation, at least in part, through NF-κB/IκBα and HIF-1α signaling pathway in LPS-induced lung inflammation.

In summary, this study has provided a new concept in the pathogenesis of LPS-induced lung inflammation, which is associated with ER stress that may be one of promising therapeutic targets for LPS-related diseases.

Methods

Animals and experimental protocol. Female C57BL/6 mice, 7 to 8 weeks of age and free of murine specific pathogens, were obtained from the Orient Bio Inc. (Seoungnam, Korea), were housed throughout the experiments in a laminar flow cabinet, and were maintained on standard laboratory chow *ad libitum*. All experimental animals used in this study were under a protocol approved by the Institutional Animal Care and Use Committee of the Chonbuk National University (Jeonju, Korea). Mice were treated once by intratracheal instillation with 50 μg of lipopolysaccharide (LPS) (Sigma-Aldrich, St Louis, MO) in 50 μl saline (or with saline as a control) under anesthesia using inhaled isoflurane (Matrix, Orchard Park, NY). Bronchoalveolar lavage (BAL) was performed at 48 hours after treatment of LPS. At the time of lavage, the mice (8 mice in each group) were sacrificed by cervical dislocation. The chest cavity was exposed to allow for expansion, after which the trachea was carefully intubated. Prewarmed 0.9% NaCl solution was slowly infused into the lung and withdrawn. The collected solutions were pooled and then kept at 4°C. A part of each pool was used for total cell counting. After centrifugation, the BAL supernatants were stored at −70°C until use. Cell pellets were resuspended with phosphate-buffered saline (PBS, Gibco-Invitrogen, Carlasbad, CA) for cell differentials. Total cell numbers were counted with a Nucleocounter (Chemometec.,Gydevang, Denmark). Smears of BAL cells were prepared by cytospin (Thermo Electron, Waltham, MA), and stained with Diff-Quik solution (Dade Diagnostics of Puerto Rico Inc., Aguada, Puerto Rico) in order to examine cell differentials. At least 400 cells were counted on each of four different corners using a microscope.

Cell culture and treatment. Normal human bronchial epithelial (NHBE) cells were purchased from Lonza (Walkersville, Md). The cells were cultured in bronchial epithelial basal medium (BEBM, Lonza) supplemented with 10% (v/v) FBS (Lonza), bovine pituitary extract, gentamicin, amphotericin B, hydrocortisone, epidermal growth factor, epinephrine, insulin, triiodothyronine, transferrin, and retinoic acid, which were maintained in a humidified incubator of 5% CO_2 atmosphere at 37°C. Cells were seeded in culture dishes and grown until 70% confluence. The medium was then replaced with a new basal medium containing vehicle (phosphate buffered saline; PBS) or 10 mmol/L sodium 4-phenylbultyrate (PBA) (Calbiochem, San Diego, CA) 1 hour before LPS stimulation. The cells were pre-activated with 50 ng/ml of TNF-α and then stimulated with 100 μg/ml of LPS in the presence or absence of 4-PBA for 12 hours. Cells were harvested and extracted.

Transfections with siRNA. RNA interference was performed with three pools of GRP78 siRNA or negative control siRNA (Santa Cruz Biotechnology, Santa Cruz, CA). siRNAs (80 nM) were transfected to NHBE cells grown until 60% confluence. At 7 hours after the transfections, 2-times concentrated growth medium was added to the plates without removing the transfection mixture and further incubated for 18 hours. The medium was then replaced with normal growth medium. After additional incubation for 12 hours, cells were stimulated with LPS. The sequences of siRNA were as follows: human GRP78, A, 5′- CUCUGGUGAUCAAGAUACAtt-3′ (sense); B, 5′-CAAGGUCUAUGAAGGUGAAtt-3′ (sense); C, 5′-GGAAAGCUAU GCCUA-UUCUtt-3′ (sense).

Isolation of peripheral blood mononuclear cells (PBMCs). Heparinized venous blood was obtained from healthy volunteers and patients with severe lung inflammation in accordance with a protocol approved by the Institutional Review Board for Chonbuk National University Hospital. Fully informed written consent was obtained from each subject. PBMCs were isolated using dextran sedimentation and Hypaque-Ficoll density-gradient separation followed by hypotonic lysis of erythrocytes as previously described[33,34]. Generally monocytes comprise approximately 10% of the isolated PBMCs. Purified PBMC were resuspended in PBS and kept on ice until use.

Administration of 4-PBA. 4-PBA (200 mg/kg of body weight) dissolved in PBS was administered through intraperitoneally 4 times to each animal 1 hour before the LPS treatment and at 6, 18, and 24 hours after the LPS treatment.

Protein determination in BAL fluid. BAL total protein amounts were determined using BAL supernatant according to the method of Bradford (Bio-Rad Laboratories, Hercules, CA).

Measurement of plasma exudation. To assess lung permeability, Evans blue dye (EBD; Sigma-Aldrich) solution (5 mg/ml) was injected into the tail vein at a concentration of 50 mg/kg. After 30 minutes, the animals were sacrificed and their chests were opened. Normal saline containing 5 mmol/L EDTA was perfused through the aorta until all venous fluid returned to the opened right atrium was clear. Lungs were carefully excised and weighed wet. EBD was extracted in 2 ml formamide kept in a water bath at 60°C for 3 hours, and the samples were centrifuged at 500 *g* for 10 minutes. The absorption of light at 595 nm was measured spectrophotometrically (Microplate reader, Bio-Rad Laboratories) with the supernatants. The dye extracted was quantified by interpolation against a standard curve of dye concentration in the range of 0.01–10 μg/ml and is expressed as ng of dye/mg of wet lung.

Histology. At 48 hours after the LPS treatment, mice were euthanized for histological assessment. Lung and trachea of mice were removed from the mice, and then for fixation, 10% (v/v) neutral buffered formalin was used. Specimens were dehydrated and embedded in paraffin. For histological examination, 4-μm sections of fixed embedded tissues were cut on a Leica model 2165 rotary microtome (Leica Microsystem Nussloch GmbH, Wetzlar, Germany), placed on glass slides, deparaffinized, and stained sequentially with H&E (Richard-Allan Scientific, Kalamazoo, MI). Stained tissue sections on slides were analyzed under identical light microscope (Axio Imager M1, Karl Zeiss, Germany) conditions, including magnification (×10), gain, camera position, and background illumination.

Immunofluorescence staining for GRP78 and CHOP. Paraffin-embedded lung tissue sections were deparaffinized and hydrated. After antigen retrieval, the tissues were fixed with 2% paraformaldehyde (Sigma-Aldrich) in PBS, and permeabilized with 0.1% Triton X-100 (Sigma-Aldrich) in PBS. After blocking with 2% bovine serum albumin (BSA, Sigma-Aldrich) in PBS for 1 hour, they were probed with an anti-GRP78 antibody (Santa Cruz Biotechnology [Catalog No. sc1050]), anti-CHOP antibody (Santa Cruz Biotechnology [Catalog No. sc166682]), and each isotype control antibody (Santa Cruz Biotechnology [Catalog No. sc2028 (GRP78), sc2025 (CHOP)]). The slides were then stained with Alexa Fluor 488 (green) or Alexa Fluor 546 (red) conjugated secondary antibodies (Invitrogen, Carlasbad, CA [Catalog No. A11055, A11003]) for detection of GRP78 and CHOP, respectively. For identification of nuclei, the fluorescent nucleic acid dye DAPI (Invitrogen) was applied for 10 minutes. Stained tissues were mounted on slides using fluorescent mounting medium (Golden Bridge International, Inc., Mukilteo, WA), and then visualized using a confocal microscope (Zeiss LSM 510 Meta, Karl Zeiss) equipped with a C-Apochromat 63×/1.20 W Korr UV-VIS-IR M27 water immersion objective.

Micro-computed tomography (CT). The lung of each mouse was scanned with a high resolution *in vivo* micro-CT system for small animal imaging (Skyscan 1076, Kontich, Belgium) at 48 hours after LPS or saline treatment. During the scan, mouse was lying on a computer-controlled rotation holder and scanned over a total rotation of 360° in rotation steps of 0.6°. Microfocus X-ray tube was operated at a voltage of 48 kV and a current of 200 μA. The exposure time for each of one image was 0.3 seconds. Acquired images were reconstructed with NRecon program (Skyscan) by using Feldkamp back projection algorithm, resulting in approximately 600 continuous scan images. Image analysis was performed with DataViewer software version 1.4.3 (Skyscan), a 3D-rendering program package.

Western blot analysis. Protein levels were analyzed by Western blotting, as described previously[5,25]. The blots were probed with an anti-GRP78 antibody (Cell Signaling Technologies, Beverly, MA [Catalog No. 3183]), anti-CHOP antibody (Santa Cruz Biotechnology [Catalog No. sc166682]), anti-phospho-eIF2α (Ser51) antibody (Cell Signaling Technologies [Catalog No. 9721]), anti-eIF2α antibody (Cell Signaling Technologies [Catalog No. 9722]), anti-VEGF antibody (Santa Cruz Biotechnology [Catalog No. sc507]), anti-ICAM-1 antibody (Santa Cruz Biotechnology [Catalog No. sc18853]), anti-KC antibody (R&D systems, Inc., Minneapolis, MN [Catalog No. MAB453]), anti-IFN-γ antibody (Santa Cruz Biotechnology [Catalog No. sc59992), anti-TNF-α antibody (Thermo Fisher Scientific Inc., Rockford, IL [Catalog No. MM350C]), anti-IL-1β (Thermo Fisher Scientific Inc. [Catalog No. MM425B]), anti-IκB-α antibody (Cell Signaling Technologies [Catalog No. 4812]), anti-lamin B antibody (Santa Cruz Biotechnology [Catalog No. sc6216]), or anti-actin antibody (Sigma-Aldrich). Anti-rabbit (Catalog No. 7074) or anti-mouse (Catalog No. 7076) horseradish peroxidase (HRP)-conjugated secondary antibodies (Cell Signaling Technologies) and anti-goat (Catalog No. sc2020) or anti-rat (Catalog No. sc2006) HRP-conjugated secondary antibodies (Santa Cruz Biotechnology) were used to detect binding of antibodies. The binding of the specific antibody was visualized by exposing to a photographic film after treating with enhanced chemiluminescence system reagents (GE Healthcare, Little Chalfont, Buckinghamshire, UK). The film was scanned and quantified using the quantification software (GS 800, Bio-Rad Laboratories). For the quantification of specific bands, the same size square was drawn around each band to measure the intensity and then the value was adjusted by the intensity of the background near that band. The results were expressed as a relative ratio of the target protein to reference protein. The relative ratio of the target protein of control group is arbitrarily presented as 1.

Cytosolic or nuclear protein extraction for analysis of transcription factors. Cytosolic or nuclear extraction was performed as described previously[5,25]. The levels of proteins were analyzed by Western blotting using antibodies against XBP-1 (Santa Cruz Biotechnology [Catalog No. sc7160]), ATF-4 (Santa Cruz Biotechnology [Catalog No. sc7583]), ATF-6 (Santa Cruz Biotechnology [Catalog No. sc22799]), HIF-1α (R&D systems [Catalog No. MAB1536]), HIF-1β (Cell Signaling Technologies [Catalog No. 3718]), or NF-κB p65 (Millipore Corporation, Billerica, MA [Catalog No. 06-418]) as described above.

Statistical analysis. We used SPSS statistical software (version 16.0, SPSS, Chicago, IL). Data were expressed as mean ± SEM. Statistical comparisons were performed using one-way ANOVA followed by the Scheffe's test. Statistical differences between two groups were determined using the unpaired Student's *t* test. A value of $P < 0.05$ was considered statistically significant.

1. Ulich, T. R. *et al.* Intratracheal injection of LPS and cytokines. V. LPS induces expression of LIF and LIF inhibits acute inflammation. *Am. J. Physiol.* **267**, L442–446 (1994).
2. Blackwell, T. S. & Christman, J. W. The role of nuclear factor-kappa B in cytokine gene regulation. *Am. J. Respir. Cell Mol. Biol.* **17**, 3–9 (1997).
3. Fan, J., Ye, R. D. & Malik, A. B. Transcriptional mechanisms of acute lung injury. *Am. J. Physiol. Lung Cell. Mol. Physiol.* **281**, L1037–1050 (2001).
4. Kuschel, A., Simon, P. & Tug, S. Functional regulation of HIF-1α under normoxia—is there more than post-translational regulation? *J. Cell. Physiol.* **227**, 514–524 (2012).
5. Lee, K. S. *et al.* Hydrogen peroxide induces vascular permeability via regulation of vascular endothelial growth factor. *Am. J. Respir. Cell Mol. Biol.* **35**, 190–197 (2006).
6. Ron, D. & Walter, P. Signal integration in the endoplasmic reticulum unfolded protein response. *Nat. Rev. Mol .Cell Biol.* **8**, 519–529 (2007).
7. Hosoi, T. & Ozawa, K. Endoplasmic reticulum stress in disease: mechanisms and therapeutic opportunities. *Clin. Sci (Lond).* **118**, 19–29 (2010).
8. Hotamisligil, G. S. Endoplasmic reticulum stress and the inflammatory basis of metabolic disease. *Cell* **140**, 900–917 (2010).
9. Zhang, K. & Kaufman, R. J. From endoplasmic-reticulum stress to the inflammatory response. *Nature* **454**, 455–462 (2008).
10. Li, J., Wang, J. J., Yu, Q., Wang, M. & Zhang, S. X. Endoplasmic reticulum stress is implicated in retinal inflammation and diabetic retinopathy. *FEBS Lett.* **583**, 1521–1527 (2009).
11. Endo, M., Mori, M., Akira, S. & Gotoh, T. C/EBP homologous protein (CHOP) is crucial for the induction of caspase-11 and the pathogenesis of lipopolysaccharide-induced inflammation. *J. Immunol.* **176**, 6245–6253 (2006).

12. Nakayama, Y. *et al.* Molecular mechanisms of the LPS-induced non-apoptotic ER stress-CHOP pathway. *J. Biochem.* **147**, 471–483 (2010).
13. Malhotra, D. *et al.* Heightened endoplasmic reticulum stress in the lungs of patients with chronic obstructive pulmonary disease: the role of Nrf2-regulated proteasomal activity. *Am. J. Respir. Crit. Care Med.* **180**, 1196–1207 (2009).
14. Korfei, M. *et al.* Epithelial endoplasmic reticulum stress and apoptosis in sporadic idiopathic pulmonary fibrosis. *Am. J. Respir. Crit. Care Med.* **178**, 838–846 (2008).
15. Welch, W. J. & Brown, C. R. Influence of molecular and chemical chaperones on protein folding. *Cell Stress Chaperones* **1**, 109–115 (1996).
16. Ozcan, U. *et al.* Chemical chaperones reduce ER stress and restore glucose homeostasis in a mouse model of type 2 diabetes. *Science* **313**, 1137–1140 (2006).
17. Engin, F. & Hotamisligil, G. S. Restoring endoplasmic reticulum function by chemical chaperones: an emerging therapeutic approach for metabolic diseases. *Diabetes Obes. Metab.* **12**, 108–115 (2010).
18. Rubenstein, R. C., Egan, M. E. & Zeitlin, P. L. In vitro pharmacologic restoration of CFTR-mediated chloride transport with sodium 4-phenylbutyrate in cystic fibrosis epithelial cells containing delta F508-CFTR. *J. Clin. Invest.* **100**, 2457–2465 (1997).
19. Srinivasan, K. & Sharma, S. S. Sodium phenylbutyrate ameliorates focal cerebral ischemic/reperfusion injury associated with comorbid type 2 diabetes by reducing endoplasmic reticulum stress and DNA fragmentation. *Behav. Brain Res.* **225**, 110–116 (2011).
20. Vilatoba, M. *et al.* Sodium 4-phenylbutyrate protects against liver ischemia reperfusion injury by inhibition of endoplasmic reticulum-stress mediated apoptosis. *Surgery* **138**, 342–351 (2005).
21. Mizukami, T. *et al.* Sodium 4-phenylbutyrate protects against spinal cord ischemia by inhibition of endoplasmic reticulum stress. *J. Vasc. Surg.* **52**, 1580–1586 (2010).
22. Hayden, M. S., West, A. P. & Ghosh, S. NF-kappaB and the immune response. *Oncogene* **25**, 6758–6780 (2006).
23. Opitz, B., van Laak, V., Eitel, J. & Suttorp, N. Innate immune recognition in infectious and noninfectious diseases of the lung. *Am. J. Respir. Crit. Care Med.* **181**, 1294–1309 (2010).
24. Schmidt, D. *et al.* Critical role for NF-kappaB-induced JunB in VEGF regulation and tumor angiogenesis. *EMBO J.* **26**, 710–719 (2007).
25. Lee, K. S. *et al.* Peroxisome proliferator activated receptor-gamma modulates reactive oxygen species generation and activation of nuclear factor-kappaB and hypoxia-inducible factor 1alpha in allergic airway disease of mice. *J. Allergy Clin. Immunol.* **118**, 120–127 (2006).
26. Semenza, G. L. Hypoxia-inducible factor 1: master regulator of O2 homeostasis. *Curr. Opin. Genet. Dev.* **8**, 588–594 (1998).
27. Jung, Y. J., Isaacs, J. S., Lee, S., Trepel, J. & Neckers, L. IL-1beta-mediated up-regulation of HIF-1alpha via an NFkappaB/COX-2 pathway identifies HIF-1 as a critical link between inflammation and oncogenesis. *FASEB J.* **17**, 2115–2117 (2003).
28. Peyssonnaux, C. *et al.* Cutting edge: Essential role of hypoxia inducible factor-1alpha in development of lipopolysaccharide-induced sepsis. *J. Immunol.* **178**, 7516–7519 (2007).
29. Werno, C., Zhou, J. & Brüne, B. A23187, ionomycin and thapsigargin upregulate mRNA of HIF-1alpha via endoplasmic reticulum stress rather than a rise in intracellular calcium. *J. Cell. Physiol.* **215**, 708–714 (2008).
30. Chen, D., Thomas, E. L. & Kapahi, P. HIF-1 modulates dietary restriction-mediated lifespan extension via IRE-1 in Caenorhabditis elegans. *PLoS Genet.* **5** (5) e1000486 (2009). doi:10.1371/journal.pgen.1000486.
31. Lee, Y. C., Kwak, Y. G. & Song, C. H. Contribution of vascular endothelial growth factor to airway hyperresponsiveness and inflammation in a murine model of toluene diisocyanate-induced asthma. *J. Immunol.* **168**, 3595–3600 (2002).
32. Lee, C. G. *et al.* Vascular endothelial growth factor (VEGF) induces remodeling and enhances TH2-mediated sensitization and inflammation in the lung. *Nat. Med.* **10**, 1095–1103 (2004).
33. Blomkalns, A. L. *et al.* Low level bacterial endotoxin activates two distinct signaling pathways in human peripheral blood mononuclear cells. *J. Inflamm (Lond).* **8**, 4 (2011). doi:10.1186/1476-9255-8-4.
34. Böyum, A. Isolation of mononuclear cells and granulocytes from human blood. Isolation of monuclear cells by one centrifugation, and of granulocytes by combining centrifugation and sedimentation at 1 g. *Scand. J. Clin. Lab. Invest. Suppl.* **97**, 77–89 (1968).

Acknowledgments

We thank Professor Mie-Jae Im for critical readings of the manuscript.

Author contributions

Kim H.J. performed experiments and analyzed data; Jeong J.S. wrote the manuscript and analyzed data; Kim S.R. designed research, interpreted data, and edited manuscript; Park S.Y. analyzed data and reviewed the manuscript; Chae H.J. reviewed the manuscript; Lee Y.C. designed research, interpreted data, and edited the manuscript.

Additional information

Supplementary information accompanies this paper at http://www.nature.com/scientificreports

Competing financial interests: The authors declare no competing financial interests.

How to cite this article: Kim, H.J. *et al.* Inhibition of endoplasmic reticulum stress alleviates lipopolysaccharide-induced lung inflammation through modulation of NF-κB/HIF-1α signaling pathway. *Sci. Rep.* **3**, 1142; DOI:10.1038/srep01142 (2013).